Journal of Cleaner Production 434 (2024) 139690

Contents lists available at ScienceDirect

Journal of Cleaner Production

journal homepage: www.elsevier.com/locate/jclepro

Developing particle-based models to predict solar energy attenuation using long-term daily remote and local measurements

Masoud Mardani [a], Siamak Hoseinzadeh [b,*], Davide Astiaso Garcia [b]

[a] Department of Energy, Materials and Energy Research Center (MERC), P.O. Box: 14155-4777, Tehran, Iran
[b] Department of Planning, Design, and Technology of Architecture Sapienza University of Rome, Rome 00196, Italy

ARTICLE INFO

Handling Editor: Panos Seferlis

Keywords:
Aerosols
Energy and environment analysis
Feasibility study
Solar energy
Solar mapping
Pollution

ABSTRACT

Iran has an annual average of 2.8–5.4 kW h/m^{2}d of radiation and has a high capacity for extracting electricity from its solar resources. Tehran, the capital of Iran, is one of the most polluted cities in the world in terms of atmospheric aerosols. Due to the rising air pollution in Tehran, the existing research is outdated. An analysis of the loss of electricity generation due to particulates can significantly affect the feasibility of a photovoltaic power plant in Tehran. Several factors affect the electricity generation of photovoltaic systems. The most critical is solar radiation. The amount of solar radiation transmitted and, ultimately, the amount of electricity generated depends on several atmospheric factors. One of the most important factors is the concentration of suspended particles of different sizes. In the present work, linear models based on observed suspended particle concentrations, including PM10 and PM2.5, have been proposed for Tehran from 2014 to 2020 to anticipate the aerosol attenuation index due to aerosols. Based on the correlation coefficient values (R), in the first and last months of the year, November, December, and January, the models performed better to predict the aerosol attenuation index based on PM2.5. The R values were, in order, 0.1553, 0.2926, and 0.1341. As remote measurements, the NASA CERES syn 1-deg product parameters and, as ground observations, Surface Solar Radiation (SSR) and PM10 and PM2.5 concentrations were used to estimate the impacts of aerosols on radiation. With the help of the CERES syn 1-deg product, it is declared that, on average, 8.30% of the total radiation received was wasted due to the presence of aerosols. Considering observed SSR, CERES syn 1-deg product performance was validated, with RMSE and MBD values of 14.09% and 10.89%, respectively.

1. Introduction

1.1. Background on the importance of solar energy for renewable energy systems

The demand for energy is increasing due to population growth, technological advancements, and industry, highlighting the need for renewable energy sources (Khan et al., 2018). By 2050, energy consumption is projected to grow by nearly 50% (Kahan, 2019). Solar photovoltaic technology is a common choice for large-scale electricity generation (Maleki et al., 2021). Atmospheric factors can affect solar radiation transmission (Jiang et al., 2023a). From the mid-20th century to the 1980s, there was a gradual decrease in radiation known as "global dimming." This was caused by factors such as low cloud coverage, air quality, and atmospheric composition (Jiang et al., 2023b).

1.2. Need for particle-based models in predicting solar energy attenuation

Tehran, the capital of Iran, faces severe air pollution issues (Hanafizadeh et al., 2016). It is ranked as one of the most polluted cities in the world (Heger, 2018). Tehran has a high potential for solar energy generation, receiving much more solar energy than cities like Berlin, a sustainable city (Di Matteo et al., 2017). Tehran receives 5.267 kW h/m^{2}d of solar energy, almost twice as much as Berlin (Global Solar Atlas). The transition to a solar city is crucial given the energy demand and air pollution concerns (Assareh et al., 2023). *Short-term forecasts* (Kanase-Patil et al., 2020)*—primarily, particle-based radiation models—are essential for stable energy supply and assessing the feasibility of photovoltaic power plants* (Dehghani-Sanij et al., 2023).

* Corresponding author.
E-mail addresses: hoseinzadeh.siamak@gmail.com, siamak.hosseinzadeh@uniroma1.it (S. Hoseinzadeh).

https://doi.org/10.1016/j.jclepro.2023.139690
Received 18 September 2023; Received in revised form 28 October 2023; Accepted 7 November 2023
Available online 18 November 2023

Nomenclature

GHI	Global horizontal irradiance (W/m^2)
DNI	Direct normal irradiance (W/m^2)
DHI	Diffuse horizontal irradiance (W/m^2)
SSR	Surface Solar Radiation (W/m^2)
SH	Sunshine Hours (hour)
AQI	Air Quality Index (Dimensionless)
AQCC	Tehran Air Quality Control Company
WHO	World Health Organization
MERC	Materials and Energy Research Center
PM10	Coarse particulate matter, which is 10 μm or less in diameter. (ug/m^3)
PM2.5	Fine particulate matter which, is 2.5 μm or less in diameter. (ug/m^3)
RMSE	Root Mean Square Error or Root Mean Square Deviation
RRMSE	Relative Root Mean Square Error
NRMSE	Normalized Root Mean Square Error
R	Correlation Coefficient
MBD	Mean Bias Deviation
MAE	Mean Absolute Error
MAPE	Mean Absolute Percentage Error
SD	Standard Deviation

Subscripts

R_s	Initial Surface Shortwave Down Flux (Wh/m^{2}d)
$R_{s,\ as}$	Initial Surface Shortwave Down Flux (all-sky condition, daily means) or ini_sfc_sw_down_all (Wh/m^{2}d)
$R_{s,\ na}$	Initial Surface Shortwave Down Flux (no aerosol condition, daily means) or ini_sfc_sw_down_naer (Wh/m^{2}d)
K_{aa}	Aerosol Attenuation index (Dimensionless)
$K_{aa}^{'}$	Cumulative Aerosol Attenuation index (Dimensionless)
K_{PM10}	PM10 index (Dimensionless)
$K_{PM2.5}$	PM2.5 index (Dimensionless)

Table 1
Summary of existing particle-based models used in other fields

Authors	Model type	Data type	Model elements	Step size	Period	Area
Préndez et al. (1995) (Préndez et al., 1995)	Linear	Locally observed	*DHI, GHI*, Total Suspended Particles (TSP), Air Temperature	Monthly average	1978–1988	Chile
Yang et al. (2016) (Yang et al., 2016a)	Linear	Locally observed, satellite-based	AOD, *DNI*, PM2.5, Visibility, Relative Humidity (R_H), cloud coverage, Maximum surface ground temperature (SGT)	Daily average	2004–2014 and 1993–2003	China
Yang et al. (2016) (Yang et al., 2016b)	Linear	Locally observed	Wind Speed, *GHI*, PM2.5, visibility	Hourly average	2014	China
Luo et al. (2019) (Luo et al., 2019)	Linear	Locally observed	visibility, AQI, PM_{10}, $PM_{2.5}$, *GHI, DNI, DHI*	Daily average	2016–2017	China
Zhao et al. (2019) (Zhao et al., 2019)	Non-linear, Linear	Locally observed	AQI, *Clearness Index* (K_t)	Daily average	2013–2017	China
Zhang et al. (2020) (Zhang et al., 2020)	Linear	Locally observed	*Clearness Index Attenuation* (K_d), AQI	Daily average	2014–2016	China
Yang et al. (2022) (Yang et al., 2022)	Linear	Locally observed	*DHI, GHI, Clearness Index* (K_t), AQI	Daily average	2014–2020	China
Gómez et al. (2023) (Gómez et al., 2023)	–	Locally observed	NOx, SO2, PM2.5, PM10, *GHI*, Wind Speed, Wind Direction	Monthly average	2010–2020	Spain

1.3. Literature review

1.3.1. Review of the importance and different applications of solar energy

In 2018, Sansaniwal et al. recognized that solar energy is a dependable, cost-effective, and sustainable alternative to address climate change and the rapidly decreasing fossil fuels that contribute to global warming. Its incorporation into a range of applications—including power generation, air conditioning, and solar drying—offers practical suggestions for the efficacy and energy efficiency of thermodynamics-based processes (Sansaniwal et al., 2018).

In 2018, Shahsavari and Akbari conducted research on how using solar energy, particularly solar photovoltaic (PV), can lower greenhouse gas emissions and air pollution in developing countries. They declared that by 2030, CO2, NOx, and SOx emissions can be decreased by using PV systems in place of kerosene and firewood. Solar energy provides a renewable response to energy poverty and environmental issues, despite obstacles (Shahsavari et al., 2018).

In 2021, Sengupta et al. conducted research on the dependability of solar resources, which is crucial for numerous solar energy applications, including photovoltaics, solar thermal and cooling, and concentrated solar power. In order to integrate solar energy sources, ensure grid stability, and guarantee the dependability of the solar resource and its possible applications, accurate financial analysis and distributed photovoltaic integration are crucial (Sengupta et al., 2021).

1.3.2. Review of previous studies on solar radiation prediction models

In 2014, Voyant et al. created a 2-D time series of solar radiation using Heliosat-2 model and ANN, with scaled persistence forecasting the best results in winter and spring, simple persistence in autumn (95.3%), and ANN in summer (99.8%) (Voyant et al., 2014).

In 2014, Bojanowski et al. proposed using the ERA-Interim reanalysis data to compare LSA-SAF and CM-SAF solar radiation datasets for Europe, finding an average root mean square (RMS) difference of 2 MJ/m^2 and a mean difference of 0.37 MJ/m^2 (Bojanowski et al., 2014).

In 2020, Li et al. developed a hybrid algorithm using PCA, wavelet transform analysis, and ANN to forecast daily surface solar radiation for Reunion Island in 2020, with an acceptable RMSE of 30.98 W/m^2 (Li et al., 2019).

In 2020, Yang and Bright evaluated the performance of eight models and databases, with Solcast model having the highest performance in evaluating RMSE (Yang et al., 2020).

In 2021, All-Hajj et al. conducted a comparison of several stacking-based ensembles of data-driven machine learning predictors to determine the optimal clustering techniques for combining predictors of solar radiation. The majority of the tested models were shown to be able to estimate solar radiation, but those that included merging heterogeneous models with neural meta-models performed better (Al-Hajj et al., 2021).

In 2022, Cao et al. validated data from radiation databases in China, finding that CERES-SYN1deg and SARAH-E performed better than ERA5 and MERRA-2 in anticipating GHI, with an RMSE of 19.32% and

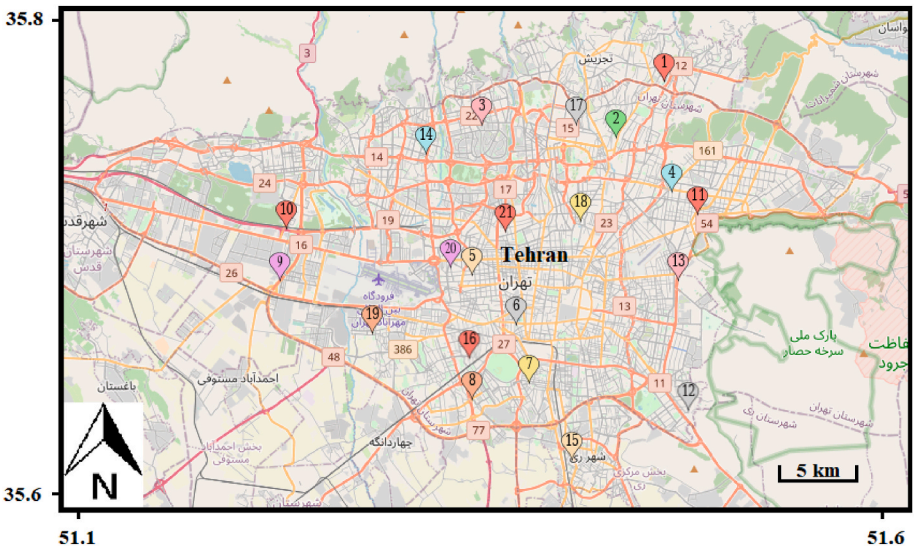

Fig. 1. The location of 21 stations of Tehran Air Quality Control Company (Tehran's Air Quality Control Company). (For interpretation of the references to color in this figure legend, the reader is referred to the Web version of this article.)

16.72%, respectively (Cao et al., 2022).

In 2022, Sun et al. investigated the impact of gridded data on clear-sky radiation models in Singapore, finding that DNI_{cs} are more responsive to AOD550 fluctuation than GHIcs (Sun et al., 2022).

1.3.3. Review of previous studies on predicting solar energy attenuation using remote sensing data

In 2019, Montesinos et al. presented a novel approach for the estimation of ground-level direct normal irradiance (DNI) in concentrated solar power (CSP) plants, considering the effects of atmospheric extinction. Comparison results indicated a normalized root-mean-square error (nRMSE) of less than 6% and strong correlation coefficients (R) above 0.94 (Alonso-Montesinos et al., 2019).

In 2021, Kay and Prasad developed a satellite model for solar energy forecasting in 2021, utilizing remote sensing data to estimate solar energy attenuation, achieving superior performance in over 50% of situations (Prasad et al., 2021).

In 2021, Dumka et al. conducted a study on atmospheric aerosols and clouds in Nainital, which revealed that atmospheric aerosols had significant impacts on solar radiation, reducing both global and beam horizontal irradiance (Dumka et al., 2021).

In 2022, Cheng et al. improved the modeling of solar radiation and attenuation effects of aerosol using the WRF-Solar model with the help of AOD data in northern China. Results showed that the direct application of satellite-based AOD data is effective in improving solar radiation modeling and investigating the attenuation effect of aerosol (Cheng et al., 2022).

In 2022, Jia et al. evaluated three machine learning models for predicting GHI and DHI under different weather conditions and air pollution. The SVM model was more reliable, with the maximum amount of error occurring in the most polluted and cleanest atmospheric conditions (Jia et al., 2022).

1.3.4. Review of existing particle-based models used in other fields (see Table 1)

In 1995, Prendez et al. studied the correlation between solar radiation, air temperature, and total suspended particulate matter (TSP) in Santiago, Chile. Results showed an agreement between TSP values and solar radiation and temperature for urban locations, with a calculated R^2 of 0.7 (Préndez et al., 1995).

In 2016, Yang et al. found that aerosol pollution (AOD provided by Modis and MISR sources) significantly affects solar radiation, with the highest amount of loss reported in Zhengzhou, and showing the absorption of radiation by aerosol is higher in the central parts of China (Yang et al., 2016a).

In 2019, Luo et al. studied the relationship between air pollution, visibility, AQI, PM2.5, and radiation changes in Nanjing, China. Results showed that PM2.5 had the most significant impact on changes in scattered radiation, with a correlation coefficient of −0.92 (Luo et al., 2019).

In 2016, Yang et al. investigated the effects of winds in heavy aerosol pollution conditions on solar radiation, and found that there are direct agreements between solar radiation and VIS, as well as between surface winds and aerosols (Yang et al., 2016b).

In 2019, Zhao et al. investigated the effects of fog and haze on solar radiation using principal component analysis (PCA) and global solar radiation weakening models (GSRW models). Results showed that in Tianjin, China, the average value of the weakening degree was 18.66%, 26.37%, 37.32%, and 45.58%. The GSRW models were validated in six other regions with different conditions of fog and haze, and their values of R-value, RMSE, and MAPE were 0.730, 0.059, and 9.430, respectively (Zhao et al., 2019).

In 2020, Zhang et al. investigated the relationship between air pollution and radiation in China, finding that the monthly clearness index attenuation showed higher values in winter than in summer. Tianjin had the highest radiation attenuation ratio at 6.56 % (Zhang et al., 2020).

In 2022, Yang et al. studied the effects of air pollution on GHI and DHI in six cities in China from 2014 to 2020. The results showed that the highest attenuation ratio was observed in spring, autumn, winter, summer, autumn, and winter, respectively. Also, the relative attenuation caused by air pollution in Beijing from 2014 to 2020 was the highest, 6.03% (Yang et al., 2022).

In 2023, Gómez et al. studied the correlation between solar radiation, air pollutants (NOx, SO2, PM2.5, and PM10) and wind fields in coastal region of Spain. Results showed high agreement between solar radiation and NOx in annual cycles (Gómez et al., 2023).

Identification of gaps in the literature and the need for a new particle-based model for solar energy attenuation prediction.

One of the first researches that investigated the effect of air pollution on the generation capacity of photovoltaic panels in Tehran dates back to 1999–2000. The research result indicated that air pollution led to a 60% decrease in electricity generation capacity in Tehran. The amount of power degradation was obtained from comparing the generated

Table 2
The description of the GHI measurement equipment used in the research (Kippb).

Observation instrument	Directional response (up to 80° with 1000 W/m^2 beam)	Operating temperature (C)	Spectral range (nm)	Spectral sensitivity	Response time	Long-term stability	Sensitivity (uV/W/m2)
Kipp & Zonen CMP-22	<5 W/m^2	−40 to +80	200–3600	<1%	<5 s	<5%	7 to 14

Table 3
CERES-SYN 1-deg product summary (Li et al., 2021).

Product	Spatial resolution	Coverage	Main input	Method
CERES SYN 1-deg	1° (~100 km)	2000–present	CERES, MODIS, GEOS-4/5, etc.	Radiative Transfer Code

electricity on December 17, 1999, and December 22, 1999 (Asl-Soleimani et al., 2001). On the other hand, Tehran is known as one of the most polluted cities in the world, especially in terms of PM2.5 pollution. In addition, Tehran has a high potential for converting electricity from solar radiation with an average received radiation of 4.5–5.2 kW h/m^{2}d (Ahmad, 2018). *So, investigating the drop in available solar irradiation due to aerosols/particles can improve the positioning of PV power plants* (Gutiérrez et al., 2018).

In the present article, considering PM2.5 and PM10 concentration values and the NASA CERES SYN 1-deg product parameters (Cao et al., 2022), precise climate data for research and modeling, from 2014 to 2020, *monthly linear correlations* between PM2.5 and PM10 and atmospheric aerosol attenuation have been proposed for Tehran *to anticipate the attenuation of solar energy due to aerosols* with the help of *locally-observed suspended particle concentrations* (Ballestrín et al., 2020). In particular, the consequences can be seen on the plane of PV panels. Hence, the feasibility study of PV power plant installation can be studied and improved by using historical time series and predicted solar radiation data simultaneously (Lopes et al., 2021).

2. Data and methods

Methods and data will be described in this section.

2.1. Observation site and datasets

Observation site and datasets will be described in this section.

2.1.1. Observation site

Tehran is the capital of Iran, with 12.5 million people and 17 million car trips planned daily. It is one of the most polluted cities in the world, ranking 12th among 26 metropolitan areas in PM10 levels (Heger, 2018). The Materials and Energy Research Center (35.748769, 50.957442) was adopted to collect GHI data from March 2014 to December 2020. No reliable data was recorded between January and June 2015 due to technical problems. Regular maintenance services were performed, and the measurement site was 25 km from the nearest air quality control station, District 21 (see Fig. 1) (Table 6).

The GHI radiation measurement sensor model CMP-22, produced by Kipp & Zonen company, was used to measure SSR. The features are presented in Table 2. Also, the sunshine duration sensor CSD3 produced by Kipp & Zonen company was used to detect days with clear sky.

Table 6
The air quality monitoring stations of Tehran AQCC (Latitude/Longitude Distance Calculator).

Index	Stations	Lat	Lon	Distance (km)
1	Aqdasiyeh	35.798863	51.484551	48
2	Darrous	35.769915	51.454108	45
3	District 2	35.776633	51.367817	37
4	District 4	35.742304	51.489826	48
5	District 10	35.699104	51.362052	37
6	District 11	35.673486	51.389766	40
7	District 16	35.643377	51.398158	41
8	District 19	35.634885	51.361983	39
9	District 21	35.696084	51.238896	25
10	District 22	35.723064	51.242733	26
11	Golbarg	35.730363	51.506106	50
12	Masoudieh	35.629859	51.499584	51
13	Piroozi	35.696169	51.49345	49
14	Punak	35.761631	51.332063	34
15	Ray	35.603958	51.425465	45
16	Rose Park	35.629859	51.499584	51
17	Sadr	35.77633	51.428433	43
18	Setad bohran	35.727051	51.430811	43
19	ShadAbad	35.668927	51.297697	32
20	Sharif University	35.703137	51.347887	36
21	Tarbiat Modares University	35.721304	51.382942	39

Table 4
CERES SYN 1-deg Ed4A Shortwave Down Flux product parameters and related supplementary information (Rutan et al., 2015)

Parameters	Abbreviations (in CERES SYN 1-deg ED4A dataset)	Abbreviations (in this article)	Effective Atmospheric Factors		
			Clouds	Aerosols	Molecular scattering and absorption
Initial Surface Shortwave Down Flux (all-sky condition, hourly means)	ini_sfc_sw_down_all_1 h	$R_{s,\ as}$	yes	yes	yes
Initial Surface Shortwave Down Flux (clear-sky condition, hourly means)	ini_sfc_sw_down_clr_1 h	–	no	yes	yes
Initial Surface Shortwave Down Flux (no aerosol condition, hourly means)	ini_sfc_sw_down_naer_1 h	$R_{s,\ na}$	yes	no	yes
Initial Surface Shortwave Down Flux (pristine condition, hourly means)	ini_sfc_sw_down_pri_1 h	–	no	no	yes

Table 5
The PM2.5 and PM10 measurement instrument used in AQCC company in Tehran.

Observation instrument	Operating temperature (C)	Measurement range (ug/m3)	Resolution (ug/m3)	Accuracy	Main flow rate (l/min)	Bypass flow rate (l/min)
TEOM-1405	−40 to +60	0–1	0.1	±75%	3	13.67

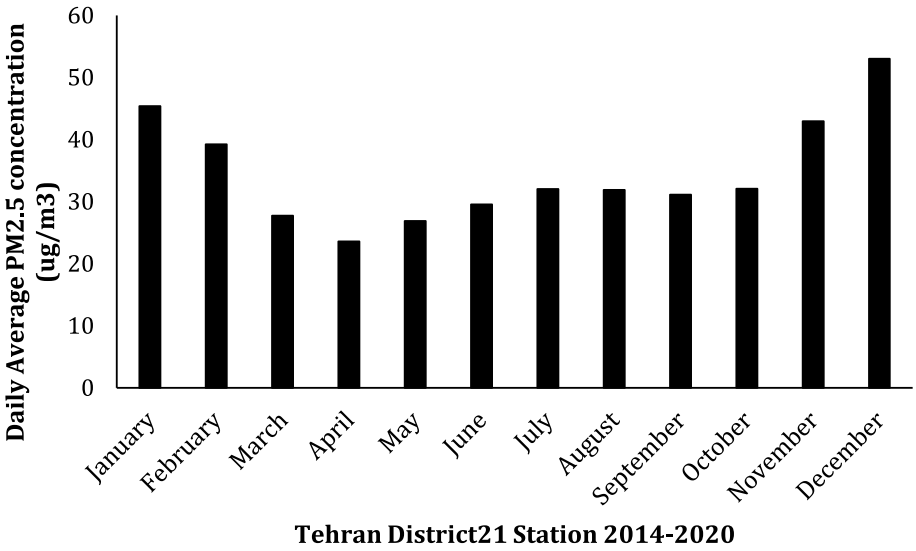

Fig. 2. Monthly variation in PM2.5 concentrations (2014–2020) at Tehran's district 21 station.

Table 7
Investigating the daily average concentrations of PM2.5 at the district 21 Station in Tehran, rearranged monthly for 2014–2020.

Period	Seasons	Sample size	Monthly Average of Daily Average PM2.5 Concentration			
			Min. (ug/m3)	Max. (ug/m3)	Mean (ug/m3)	SD (ug/m3)
2014–2020	January	168	13	94	45.38	17.02
	February	141	12	143	39.22	20.02
	March	150	6	78	27.75	13.07
	April	139	6	90	23.61	9.03
	May	152	13	67	26.88	8.29
	June	126	12	60	29.57	9.06
	July	154	14	68	32.01	9.07
	August	155	14	81	31.88	8.78
	September	149	12	52	31.13	8.13
	October	163	8	64	32.10	9.51
	November	172	7	104	42.95	17.53
	December	172	12	123	53.02	23.68

Table 8
Investigating the daily average concentrations of PM10 at the District 21 Station in Tehran, rearranged monthly for the entire period of 2014–2020.

Period	Months	Sample size	Monthly Average of Daily Average PM10 Concentration			
			Min. (ug/m3)	Max. (ug/m3)	Mean (ug/m3)	SD (ug/m3)
2014–2020	January	168	33	221	98.10	33.95
	February	141	37	364	97.59	45.73
	March	150	13	282	76.86	42.76
	April	140	19	172	67.22	28.40
	May	151	36	231	90.58	34.68
	June	126	52	245	103.24	31.97
	July	153	58	254	111.16	33.91
	August	154	57	274	102.64	28.05
	September	151	47	335	112.91	40.35
	October	185	41	191	100.19	28.68
	November	164	24	269	94.68	41.18
	December	173	24	220	105.69	38.63

Further information is in (Kippa).

2.1.2. Datasets

Datasets will be described in this section.

- *Shortwave Down Flux/modeled GHI*

In the present research, Shortwave Down Flux parameter data from NASA's CERES SYN 1-deg product was used from 2014 to 2020. The SYN 1-deg Ed4A product presents the Shortwave Down Flux parameters of solar radiation as monthly, daily, three-hourly, and hourly averages in four different scenarios. The effect of aerosol attenuation in the atmosphere can be calculated by considering the difference between all-sky and no-aerosol scenarios (Li et al., 2020). The daily cumulative data of NASA's CERES-SYN 1-deg product were used in all sections of this article; in other words, the hourly data of one day were added together and used in daily form in all the sections of the present work. Additional details about the SYN 1-deg Ed4A product from NASA CERES are provided in Table 3 and Table 4. Additionally, the used source code is accessible through GitHub (Mardani, 2022).

It is believed that to define SSR, the Shortwave Down Flux parameter is the same as GHI. In several papers, this parameter has been validated and used as GHI (Cao et al., 2022; Li et al., 2021; Rutan et al., 2015; Su et al., 2005, 2007). The accuracy evaluation process of CERES SYN 1-deg ED4A product and its parameters have been applied in several papers (Bannon, 2015; Bannon et al., 2017, 2018; Kato et al., 2020). Certainly, in section 3.2.3 of this article, the validation of one of the parameters of this product - ini_sfc_sw_down_all or $R_{s,\ as}$ - has been discussed.

2.1.3. Ground-level PM2.5 & PM10

Particulate matter includes microscopic substances suspended in air or water. The airborne particles are called aerosols. The aerosols with a diameter of less than 10 and 2.5 are called PM10 and PM2.5, respectively (Attia et al., 2022). The Air Quality Control Company (AQCC) provided average hourly and daily data of PM2.5 and PM10 concentrations in Tehran - freely available - between 2014 and 2020 (Tehran's Air Quality Control Company). Particulate matter data is collected by the Tapered Element Oscillating Microbalance (TEOM) instrument (see Table 5). However, there are other cheaper instruments to gather data (deSouza et al., 2020). All the urban stations of the mentioned company are located in Tehran (see Fig. 1) (Nabavi et al., 2019). Due to using 24-h average data in the overall and seasonal analysis stages, outlier data was not omitted. But in the phase of investigating the relationship between

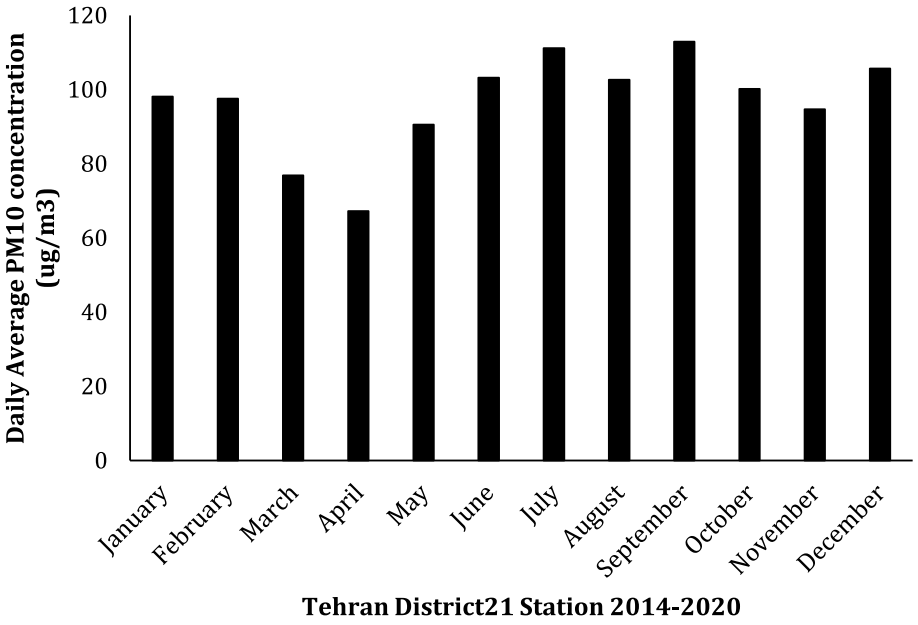

Fig. 3. Monthly variation in PM10 concentrations (2014–2020) at Tehran's district 21 station.

Table 9
Summary of the daily average concentrations of PM2.5 and PM10 in the District 21 station with the daily average concentrations of PM2.5 and PM10 in the West Area of Tehran, and the daily average concentrations of PM2.5 and PM10 in all the stations rearranged monthly in the entire period of 2014–2020.

Period	Months	Monthly Average of Daily Average PM2.5 Concentration			Monthly Average of Daily Average PM10 Concentration		
		District 21 (ug/m3)	Western Stations (ug/m3)	All the Stations (ug/m3)	District 21 (ug/m3)	Western Stations (ug/m3)	All the Stations (ug/m3)
2014–2020	January	45.38	44.35	36.92	98.10	94.09	76.83
	February	39.22	36.44	32.27	97.59	89.74	74.49
	March	27.75	27.30	24.05	76.86	74.18	58.86
	April	23.61	23.58	21.66	67.22	69.98	55.15
	May	26.88	26.36	25.002	90.58	85.30	66.95
	June	29.57	30.29	29.78	103.24	98.47	81.59
	July	32.01	33.61	30.17	111.16	108.70	86.88
	August	31.88	29.51	28.22	102.64	100.22	85.39
	September	31.13	30.07	27.81	112.91	106.12	88.07
	October	32.10	32.33	28.59	100.19	95.84	80.25
	November	42.95	42.77	35.21	94.68	93.30	76.09
	December	53.02	53.29	44.36	105.69	111.42	87.26

PM2.5 and PM10 changes and radiation loss, the outlier data were removed to improve the model's prediction accuracy. According to the AQCC's report, pollutant data is verified at air quality control stations daily at 11 a.m. and, if valid, is presented on the site and on city display boards/monitors (Tehran's Air Quality Control Company). Similar to articles (Nabavi et al., 2019) and (Liu et al., 2007), the daily average data for particulate matter were used because they had a higher agreement with the AOD. Due to the lack of PM10 and PM2.5 data measurement by five AQCC stations in Tehran in desired period, only the data of 21 stations were accessible from 2014 to 2020 (see Fig. 1). The list of stations, as well as their distances to the observation site in MERC, was presented in Table 6.

2.2. Methods

Methods will be described in this section.

2.2.1. Seasonal data classification method

For seasonal data classification, an astronomical start was used for each season instead of a meteorological start (Neshat et al., 2023).

2.2.2. Aerosol attenuation effect method

In this part, we discussed the drop resulting from aerosol with the help of parameters ini_sfc_sw_down_naer or abbreviated $R_{s,\ na}$, and ini_sfc_sw_down_all or abbreviated $R_{s,\ as}$. According to Table 4, these two parameters provide daily cumulative radiation data, including the cloud effect, and the only difference is the aerosol effect. The parameter $R_{s,\ aa}$ was expressed as the difference between the daily cumulative radiation on the earth's surface in the absence of aerosols and the daily cumulative radiation on the earth's surface in a normal state. Additionally, K_{aa} can be defined as the difference in daily cumulative radiation on the earth's surface, considering the absence of aerosols on the daily cumulative radiation on the earth's surface in normal conditions. K_{aa}' is conceptually very similar to K_{aa}, with the difference that it indicates the ratio of total $R_{s,\ aa}$ in the period to the annual total.

From now on, we will use $R_{s,\ aa}$, $R_{s,\ na}$, and $R_{s,\ as}$ parameters in the text instead of the abbreviations introduced in Table 4.

$$R_{s,as} = R_{s,na} - R_{s,as} \quad \text{Equation 1}$$

$$K_{aa} = \frac{R_{s,na} - R_{s,as}}{R_{s,as}} = \frac{R_{s,aa}}{R_{s,as}} \quad \text{Equation 2}$$

$R_{s,\ aa}$ = Solar Radiation Attenuation by Aerosol (Wh/m^{2}d).

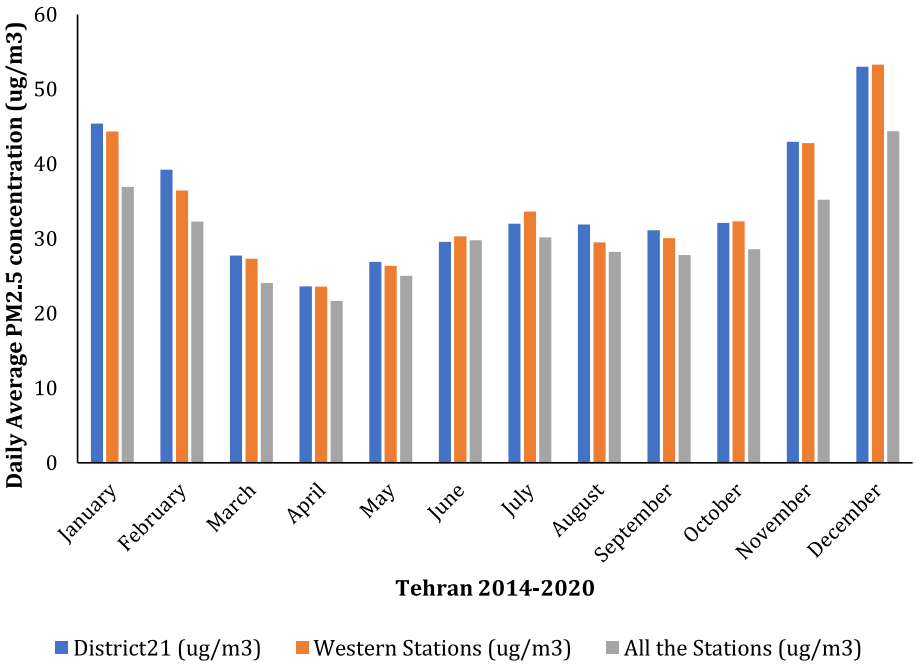

Fig. 4. Monthly comparison of PM2.5 concentrations (2014–2020) in tehran stations.

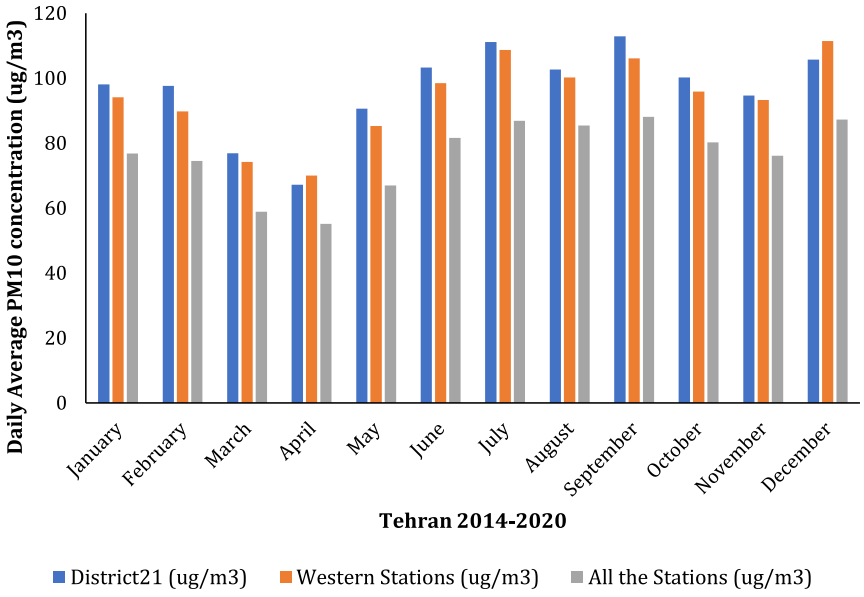

Fig. 5. Monthly comparison of PM10 concentrations (2014–2020) in tehran stations.

Table 10
Table of daily cumulative radiation data for $R_{s,\ as}$ and $R_{s,\ na}$ in the NASA CERES SYN 1-deg database for the entire 2014–2020 in Tehran.

Parameters	Total days	Min. (Wh/m^{2}d)	Max. (Wh/m^{2}d)	Mean (Wh/m^{2}d)	SD (Wh/m^{2}d)
$R_{s,\ as}$	2557	444.67	9041.02	5234.39	2174.88
$R_{s,\ na}$	2557	453.29	9463.92	5676.49	2368.45

$R_{s,\ na}$ = ini_sfc_sw_down_naer (Wh/m^{2}d).
$R_{s,\ as}$=ini_sfc_sw_down_all (Wh/m^{2}d).
K_{aa} = Aerosol Attenuation index (Dimensionless).

Table 11
Table of daily cumulative radiation for observed GHI at MERC for the entire period of 2014–2020.

Database	Total days	Min. (Wh/m^{2}d)	Max. (Wh/m^{2}d)	Mean (Wh/m^{2}d)	SD (Wh/m^{2}d)
Observed GHI in MERC	1921	199.97	7961.02	4782.146	2013.03

2.2.3. p.m.2.5 and PM10 indexing

To ease fitting linear correlations on particulate matter concentration data and aerosol attenuation, two new parameters were defined as

Table 12
Statistical properties of $R_{s,\ as}$ and SSR in MERC on clear sky days.

Database	Clear days	Min. (Wh/m^{2}d)	Max. (Wh/m^{2}d)	Mean (Wh/m^{2}d)	SD (Wh/m^{2}d)
$R_{s,\ as}$	1037	2906.7749	9041.0249	6406.9451	1758.9481
SSR or GHI	1037	1881.514	7961.025	5709.0516	1516.94

shown below:

$$K_{PM2.5} = \frac{PM2.5}{100} \quad \text{Equation 3}$$

$$K_{PM10} = \frac{PM10}{100} \quad \text{Equation 4}$$

$K_{PM2.5}$ = PM2.5 index (Dimensionless).
K_{PM10} = PM10 index (Dimensionless).

Both relationships representing the particulate matter ratios in different sizes of diameters, including PM10 and PM2.5. Both parameters are dimensionless. Due to the ease of calculations, as the authors did in (Yang et al., 2022), the $K_{PM2.5}$ was defined by dividing PM2.5 b y 100 μg/m^3 (in (Yang et al., 2022), the RAQI was calculated as a representative of the Air Quality Index as mentioned).

3. Results and discussion

3.1. Regional distribution of fine & coarse particulate matters in tehran (PM2.5 & PM10)

The purpose of this section is to offer important information into the spatial patterns of PM2.5 and PM10.

3.1.1. Regional distribution of PM2.5

Insights on PM2.5 spatial trends are sought in this section.

- *Investigating the daily average PM2.5 concentrations at the district 21 station, rearranged monthly for 2014-2020*

According to Fig. 2 and Table 7, the maximum/highest value of the daily average PM2.5 concentrations at the district 21 station from 2014 to 2020 occurred monthly in December and seasonally in the winter. On the other hand, the minimum/lowest value was in April. The maximum and minimum values were reported as 53.02 and 23.61 μg/m^3, respectively.

3.1.2. Regional distribution of PM10

Insights on PM10 spatial trends are sought in this section.

Table 13
Table of the daily cumulative radiation parameters of the daily solar radiation Shortwave Down Flux (NASA CERES syn 1-deg product) in Tehran as annual average values for the period of 2014–2020.

Year	Sample size	Yearly Average of Daily Solar Radiation Shortwave Down Flux (NASA CERES syn 1-deg)			
		$R_{s,\ na}$ (Wh/m^{2}d)	$R_{s,\ as}$ (Wh/m^{2}d)	$R_{s,\ aa}$ (Wh/m^{2}d)	K_{aa}
2014	365	5721.51	5264.45	457.05	0.0835
2015	365	5739.25	5285.43	453.82	0.0849
2016	366	5837.58	5392.89	444.68	0.0802
2017	365	5794.51	5357.08	437.42	0.0830
2018	365	5491.03	5049.11	441.92	0.0853
2019	365	5639.92	5206.57	433.35	0.0812
2020	366	5511.61	5085.20	426.40	0.0810
All data (average)	–	5703.96	5259.25	444.70	0.0830

Table 14
Table of the daily cumulative radiation parameters of the daily solar radiation Shortwave Down Flux (NASA CERES syn 1-deg product) in Tehran as annual cumulative values for the period of 2014–2020.

Years	Sample size	Yearly cumulative solar energy of Daily Solar Radiation Shortwave Down Flux (NASA CERES syn 1-deg)			
		$R_{s,\ na}$ (kWh/m^{2}d)	$R_{s,\ as}$ (kWh/m^{2}d)	$R_{s,\ aa}$ (kWh/m^{2}d)	K_{aa}
2014	365	2088.35	1921.52	166.82	0.0868
2015	365	2094.82	1929.18	165.64	0.0859
2016	366	2136.55	1973.80	162.75	0.0825
2017	365	2114.99	1955.33	159.66	0.0817
2018	365	2004.22	1842.92	161.30	0.0875
2019	365	2058.57	1900.39	158.17	0.0832
2020	366	2017.24	1861.18	156.06	0.0839
All data (Average)	–	2073.53	1912.04	161.48	0.0844
All data (Sum)	2557	14514.74	13384.32	1130.4	0.0844

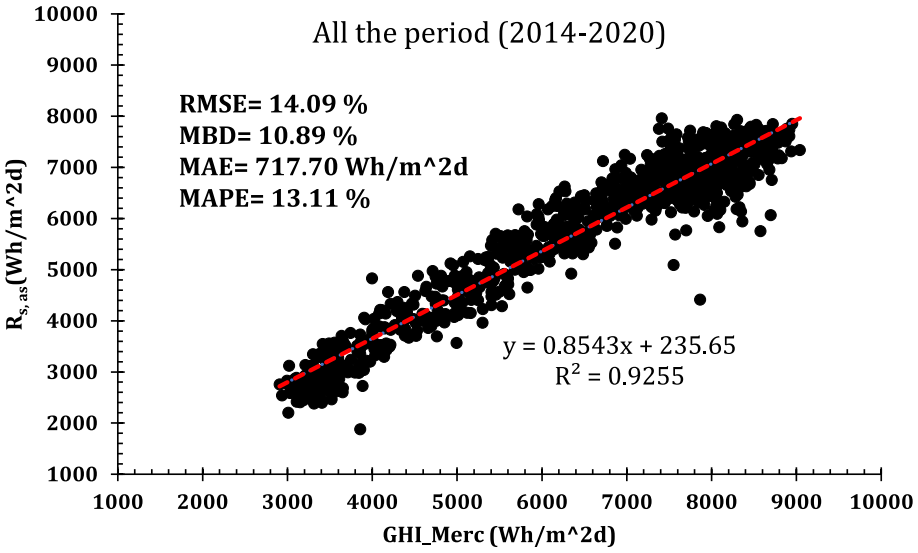

Fig. 6. Comparison of $R_{s,\ as}$ and measured GHI at MERC from 2014 to 2020 on clear-sky days.

Table 15
The table describes the minimum and maximum daily parameters of the Kaa for Tehran rearranged annually from 2014 to 2020.

Years	Data (K_{aa})	date	Daily Solar Radiation Shortwave Down Flux (NASA CERES syn 1-deg)			
			$R_{s,\ na}$ (Wh/m2d)	$R_{s,\ as}$ (Wh/m2d)	$R_{s,\ aa}$ (Wh/m2d)	K_{aa}
2014	Min.	December 26, 2014	3424.37	3405.14	19.22	0.0056
	Max.	July 02, 2014	8647.42	7310.69	1336.72	0.1828
2015	Min.	March 11, 2015	6277.59	6243.35	34.24	0.0054
	Max.	April 16, 2015	4082.54	3250.92	831.62	0.2558
2016	Min.	November 25, 2016	3886.57	3858.27	28.29	0.0073
	Max.	October 26, 2016	4137.67	3445.57	692.10	0.2008
2017	Min.	December 08, 2017	3238.45	3236.20	47.24	0.0146
	Max.	October 27, 2017	3887.57	3191.07	696.49	0.2182
2018	Min.	December 24, 2018	2563.15	2533.10	30.05	0.0118
	Max.	April 23, 2018	3367.30	2552.57	614.72	0.2233
2019	Min.	January 12, 2019	3260.17	3228.32	31.85	0.0098
	Max.	October 21, 2019	4566.34	3728.77	837.57	0.2246
2020	Min.	December 27, 2020	3301.02	3272.20	28.82	0.0088
	Max.	April 26, 2020	1996.80	1653.72	343.07	0.2074
All data	Min.	March 11, 2015	6277.59	6243.35	34.24	0.0054
	Max.	April 16, 2015	4082.54	3250.92	831.62	0.2558

Table 16
The table describes the monthly averages of the daily average cumulative solar radiation shortwave down flux values (NASA CERES syn 1-deg) in Tehran rearranged monthly for 2014–2020.

Period	Months	Sample size	Monthly Average of Daily Solar Radiation Shortwave Down Flux (NASA CERES syn 1-deg)				
			Rs, na (Wh/m2d)	Rs, as (Wh/m2d)	Rs, aa (Wh/m2d)	Kaa	Kaa'
2014–2020	January	217	3035.75	2878.56	157.19	0.0558	0.0297
	February	198	3861.53	3627.82	233.71	0.0664	0.0441
	March	217	4945.02	4592.78	352.24	0.0813	0.0665
	April	210	6167.39	5675.70	491.69	0.0930	0.0929
	May	217	7495.02	6889.42	605.60	0.0921	0.1144
	June	210	8739.42	8077.70	661.72	0.0830	0.125
	July	217	8535.79	7775.53	760.25	0.0995	0.1436
	August	217	7983.49	7356.66	626.83	0.0863	0.1184
	September	210	6712.39	6075.31	637.08	0.1061	0.1203
	October	217	4737.20	4321.35	415.84	0.0988	0.0785
	November	210	3172.31	2958.19	214.11	0.0739	0.0404
	December	217	2640.88	2502.70	138.18	0.0558	0.0261
	Sum	–	68026.19	62731.72	5294.44	–	1

In Table 16, the values of $R_{s,\ aa}$, $R_{s,\ na}$, $R_{s,\ as}$, and K_{aa} were obtained by averaging the daily cumulative values of the month for the period of 2014–2020. K_{aa}' values are defined like K_{aa}, with the difference that the sum value is placed in the fraction's denominator. In other words, this parameter expresses the ratio of the monthly drop to the total drop of whole period.

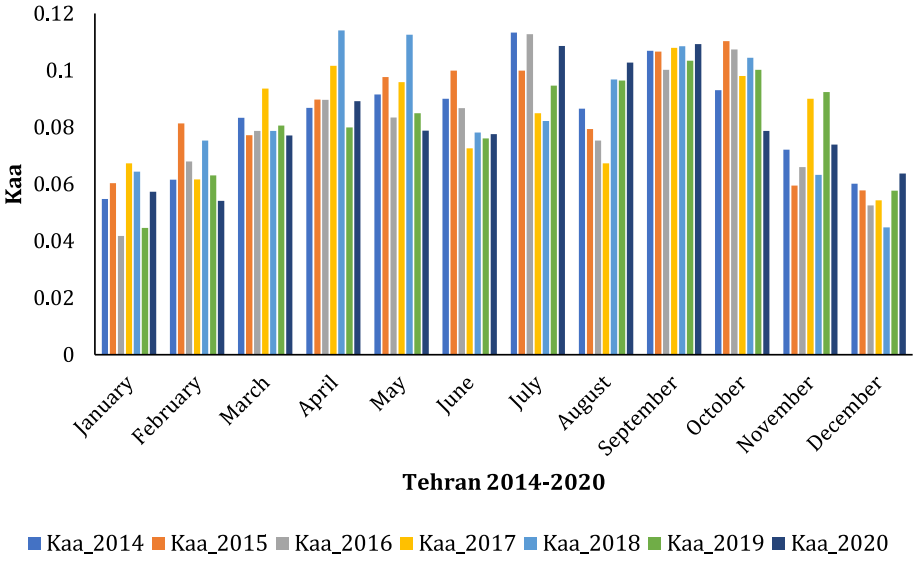

Fig. 7. Comparison of monthly Kaa values in 2014–2020.

Table 17
Description of Kaa' in Tehran for hot and cold seasons from 2014 to 2020.

Period	Seasons	Kaa'
2014–2020	Spring + Summer	0.7037
	Autumn + Winter	0.2963
	Sum	1

Table 18
The table below describes the radiation and aerosol concentration parameters in Tehran as a monthly average from 2014 to 2020.

Period	Months	AQCC (District 21)		NASA CERES syn 1-deg Product	
		PM2.5 (ug/m3)	PM10 (ug/m3)	Rs, aa (Wh/m2d)	Kaa
2014–2020	January	45.38	98.1	157.19	0.057
	February	39.22	97.59	233.71	0.054
	March	27.75	76.86	352.24	0.077
	April	23.61	67.22	491.69	0.089
	May	26.88	90.58	605.6	0.079
	June	29.57	103.24	661.72	0.078
	July	32.01	111.16	760.25	0.109
	August	31.88	102.64	626.83	0.103
	September	31.13	112.91	637.08	0.109
	October	32.1	100.19	415.84	0.079
	November	42.95	94.68	214.11	0.074
	December	53.02	105.69	138.18	0.064

- *Investigating the daily average PM10 concentrations at the district 21 station, rearranged monthly for the entire period of 2014-2020*

According to Table 8 and Fig. 3, the maximum value of the daily average PM10 concentration at the district 21 station from 2014 to 2020 occurred in September and generally in the summer. On the other hand, the minimum value was calculated in April. The maximum and minimum values were reported as 112.91 and 67.22 μg/m^3, respectively.

3.1.3. Summary of the daily averages of PM10 and PM2.5 concentrations from 2014 to 2020

By examining Table 9, the minimum value of the daily average of PM2.5 and PM10 concentrations from 2014 to 2020 occurred in April in Tehran, and their values were 21.66 and 55.15 μg/m^3, respectively. These values for the western stations occurred in April. Their values were 23.58 and 69.98 μg/m^3, respectively, and for District 21, they were 23.61 and 67.22 μg/m^3, respectively (see Figs. 4 and 5). In other words, in the seven years from 2014 to 2020, the daily average concentrations of PM2.5 and PM10 in Tehran were generally higher than 21.66 and 55.15 μg/m^3, respectively. These values were 44.4% and 22.55% higher than the WHO air quality guidelines (Organization, 2021). This indicates that air pollution in Tehran has been steadily increasing over the past several years, and that the current air quality guidelines are not adequate to protect the people of Tehran from the health risks of air pollution.

3.2. Surface solar radiation (SSR)

Surface Solar Radiation will be calculated in this section with the help of various methods.

3.2.1. Shortwave down flux (NASA CERES syn 1-deg product)

NASA's CERES syn 1-deg database provides various sub-parameters of the Shortwave Down Flux parameter in all-sky, clear-sky, and no-aerosol conditions. The statistical properties of the data illustrated in Table 4. Due to mathematical models and satellite data, the mentioned dataset was accessible on all days from 2014 to 2020 (see Table 10).

3.2.2. Observed GHI in MERC

According to the data in Table 11, to check the radiation measured in MERC, we had access to the data for 1921 days out of 2557 days between January 2014 and December 2020 (parts of the data were missed). The minimum daily amount of cumulative GHI radiation observed in MERC was 199.97 W h/m^{2}d, as expected in the winter season. On the other hand, the maximum daily value in the whole seven-year period was 7961.02 W h/m^{2}d in the spring season. This value was about 66% higher than the seven-year average daily radiation received at the desired location. Compared to previous expectations, this amount was greater than the maximum radiation received in the summer season. By default, due to the higher radiation in the summer, the maximum received radiation should be a higher value. Accordingly, the maximum average of cumulative GHI radiation received daily in 2014–2020 was in June and was 6911.38 W h/m^{2}d. On the other hand, the minimum value was in December, and it was 2219.17 W h/m^{2}d.

3.2.3. Validation of CERES SYN 1-deg rs, as with observed SSR data in merc from 2014 to 2020

In this subsection, the results of validating the radiation data obtained from observed SSR with the modeled data of NASA CERES syn 1-deg Shortwave Down Flux all sky conditions - or $R_{s,\ as}$ - will be discussed for the seven years from 2014 to 2020. To ignore the effect of clouds, the validation was done on days with clear-sky conditions.

To determine whether the sky was clear or cloudy, sky condition evaluation data from the sunshine hours data collected at the Merc was used.

Using SH, 1037 days with a clear sky condition were separated from the measurement interval from 2014 to 2020 at Merc (see Table 12). Then the shortwave down flux radiation data provided by the NASA CERES SYN 1-deg product in the all-sky condition was validated with the help of RMSE, MBD, MAE, and MAPE statistical analysis methods in these 1037 clear-sky days. For two reasons, the performance of $R_{s,\ as}$ was validated on clear-sky days. The first reason was that the focus of this paper was on the effects of aerosols and not the effects of clouds. The second reason was that the $R_{s,\ as}$ will be used in the calculations of the K_{aa}.

The measured and modeled radiation values are shown in Fig. 6. RMSE and MBD values were reported as 14.09% and 10.89%, respectively. This indicates that the model was accurate in predicting the radiation values. The RMSE and MBD values are also within the acceptable range of 20%. This suggests that the model can be used in making predictions about solar radiation.

3.3. Investigation of the changes in the daily average PM2.5 & PM10 concentrations and radiation losses from aerosols considering the SYN 1-deg product of the NASA CERES database from 2014 to 2020 in tehran

More than 99% of the sun's radiation is in the range of 0.15–4 μm (John and Duffie, 2013). This spectrum includes ultraviolet, visible, and infrared, which account for 7%, 50%, and 43% of the energy of the sun's radiation, respectively. Among atmospheric gas compounds, O_3 gas reflects and reduces available radiation in the ultraviolet spectrum. Also, water vapor absorbs and scatters radiation in the infrared spectrum. But it is more complicated for aerosols. It reduces three phenomena: reflection, scattering, and absorption. PM2.5 and PM10 often reduce radiation in the near-infrared range and, to a small extent, in the visible light range (Opálková et al., 2019).

3.3.1. Investigating the impacts of aerosols on received radiation using NASA CERES SYN 1-deg product parameters from 2014 to 2020

With the help of $R_{s,\ aa}$ we investigated the drop in received radiation due to aerosol utilizing daily cumulative radiation - introduced earlier - from 2014 to 2020.

In Table 13, the annual average values of the daily cumulative radiation of three parameters ($R_{s,\ aa}$, $R_{s,\ na}$, and $R_{s,\ as}$) from the product

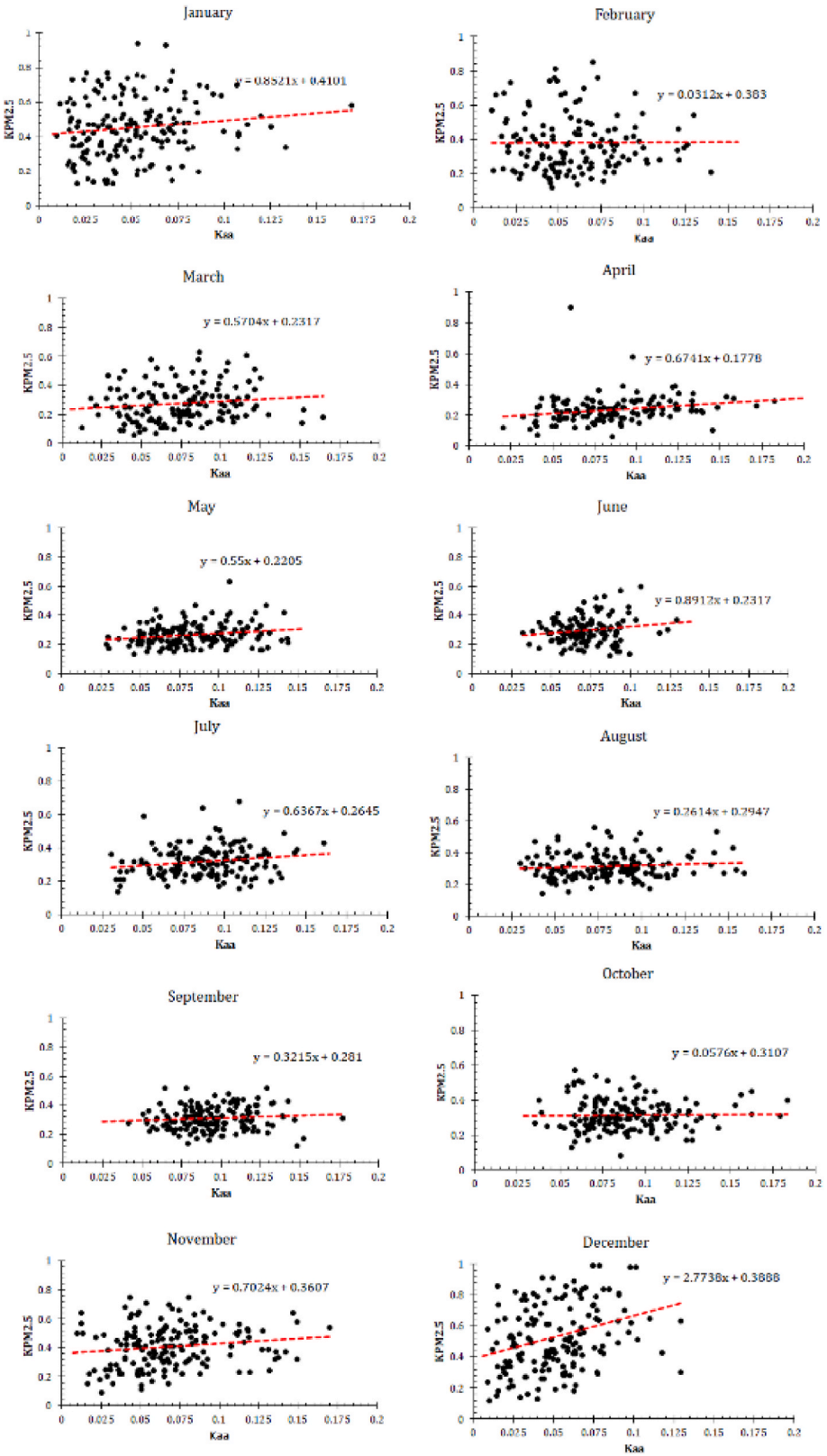

Fig. 8. The equations were fitted to the K_{aa} and $K_{PM2.5}$ rearranged monthly from 2014 to 2020.

CERES SYN 1-deg and K_{aa} are presented. As it is known, in 2018, with the value of K_{aa} equal to 0.0853, the most remarkable drop in radiation due to aerosols occurred compared to the overall received radiation. The values in the "All data (average)" section of Table 13 showed that, on average, 8.30% of the total radiation was wasted by aerosols in 2014–2020. The values in Table 14 also confirm that the largest radiation drop due to aerosols compared to the total radiation received in the seven years occurred in 2018. In this table, the values of $R_{s,\,aa}$, $R_{s,\,na}$, and $R_{s,\,as}$ have been calculated annually cumulatively, and at the end, K_{aa} has been calculated using annual cumulative values. The cumulative $R_{s,\,aa}$

Table 19
Statistical parameters and coefficients of the fitted linear models between K_{aa} and $K_{PM2.5}$ ($K_{PM2.5}$=P1*K_{aa} + P2).

Period	Months	Coefficients		Size	Correlation coefficients	RMSE (%)	MAPE (%)
		P1	P2				
2014–2020	January	0.8521	0.4104	168	0.1341	20.82	39.78
	February	0.0312	0.383	141	0.0047	17.71	8.17
	March	0.5704	0.2317	150	0.1329	21.64	23.74
	April	0.6741	0.1778	139	0.2296	9.77	26.45
	May	0.55	0.2205	151	0.1855	15.04	23.19
	June	0.8912	0.2317	126	0.1703	18.60	26.74
	July	0.6367	0.2645	154	0.1818	16.52	23.59
	August	0.2614	0.2947	154	0.0913	18.65	20.85
	September	0.3215	0.281	149	0.0920	20.25	23.68
	October	0.0576	0.3107	160	0.0173	17.92	21.34
	November	0.7024	0.3607	163	0.1553	21.33	37.29
	December	2.7738	0.3888	172	0.2926	20.40	46.29
	All data (average)	–	–	1827	0.1406	18.22	26.75

value in 2018 was 161.30 kW h/m^2d, which was unexpectedly lower than the $R_{s,\ aa}$ value in 2014, 2015, and 2016. The reason for that was the difference in $R_{s,\ as}$ value, which is placed in the denominator of the fraction in K_{aa}. Therefore, about $R_{s,\ aa}$, which shows the amount of reduced radiation due to the effect of aerosols, in Tables 13 and 14, the year 2014 has the highest reduction values from aerosols.

In Table 13, $R_{s,\ aa}$, $R_{s,\ na}$, and $R_{s,\ as}$ are the average values between the entire days of the year. Also, the value of K_{aa} for each year has been calculated by averaging the daily K_{aa}.

In Tables 14 and in contrast to Table 13, the K_{aa} has been calculated for each year by dividing the annual cumulative values. Table 15 shows the minimum and maximum values for the K_{aa} each year. According to the table, both days were from 2015. So that on April 16, 2015, 25.58% of radiation decreased due to aerosols, which was the maximum for the entire period. On the other hand, on March 11, 2015, 0.54% of the radiation decreased, which was the minimum for the whole period. In addition, on April 16, 2015 and March 11, 2015, respectively, 831.62 and 34.24 W h/m^2d of daily $R_{s,\ as}$ were wasted due to the presence of aerosols. This shows that aerosols can have a significant effect on the amount of energy that is wasted. Therefore, it is important to take measures to reduce the presence of aerosols in the atmosphere. This can be done by reducing air pollution and introducing more efficient methods of energy production (Unger, 2009).

- *Investigating the impacts of aerosols on received radiation using NASA CERES SYN 1-deg product parameters monthly from 2014 to 2020*

In Table 16, the values of $R_{s,\ aa}$, $R_{s,\ na}$, $R_{s,\ as}$, and K_{aa} were obtained by averaging the daily average values of the given month in 2014–2020. The highest radiation loss due to aerosols was observed in September, with K_{aa} of 10.61%. Aerosols reduced the daily cumulative radiation (total radiation received in one day) by 637.08 W h/m^2d in September. In both January and December, K_{aa} measured 5.58%, which is the lowest radiation loss due to aerosols. Regarding examining the K_{aa}', the highest radiation loss was evaluated in July, with a share of 14.36% of the total annual radiation loss due to aerosols. On the other hand, December was the least affected by aerosols, with a share of 2.61% of total radiation loss.

In Fig. 7, the monthly average values of K_{aa} are compared for 2014–2020. The figure shows that in February, K_{aa} values from 2014 increased until 2018 and then decreased until 2020. The K_{aa} declined throughout June from 2014 to 2020, particularly in 2018, 2019, and 2020. The trend of K_{aa} in July increased throughout the whole period. Also, in July, August, and September, the trend of K_{aa} was positive throughout the entire period. K_{aa} values rose dramatically in the last year of the period, especially in August, reaching 10.27% in 2020. In 2014, this parameter was 8.63%. In May and April of 2018, the value of the K_{aa} increased dramatically, so the values were 11.40% and 11.25%, respectively. This is a considerable increase compared to the average of the entire period of these months, which was 9.30% and 9.21%, respectively.

- *Investigating the radiation loss due to aerosols, including the phenomenon of temperature inversions, in Tehran*

A temperature inversion is a layer in the atmosphere where the air temperature increases with height. An inversion occurs at the bottom of a cap-like layer of air. The desired cap is relatively warm air above it (above the inversion layer) (What is an inversion). In 2020, Khalesi and Danehsvar investigated temperature inversions in Tehran from 2014 to 2018. It was stated that the most severe occurrences of this phenomenon happened in the winter and autumn seasons (Khalesi et al., 2020). During the temperature inversion phenomenon, pollutants from vehicles, wood burning, and industry are trapped near the ground, which leads to a severe drop in air quality. Over time and with a lack of air movement, the concentration of PM2.5 in the atmosphere increases (Cichowicz et al., 2022). To evaluate the reducing effect of aerosols in the cold seasons of the year, considering the data in advance, Table 17 was prepared. In this table, K_{aa}' values were calculated as the sum of spring and summer for hot seasons and winter and autumn for cold seasons. The results of Table 17 showed that despite the phenomenon of temperature inversions and the increase in PM2.5 concentration in the cold seasons of the year, the cold seasons had a share of 29.63% in the total radiation reduced due to aerosols in the period of 2014–2020. It means that the radiation loss due to aerosols in the hot seasons is twice as much as in the cold seasons.

The results show that maybe investing of new solutions to reduce the concentration of aerosols in the hot seasons in Tehran is much more efficient than improving the air quality in the cold seasons. Generally, in the hot seasons, PM10, which originates from the western countries of Iran (Givehchi et al., 2013), causes a decrease in radiation. Despite that, in the cold seasons, the temperature inversions and lack of air movements cause an increase in the concentration of PM2.5. It seems that the higher agreement of K_{aa} with PM2.5 or $K_{PM2.5}$ in January, October, and December, and conversely better agreement of K_{aa} with PM10 or K_{PM10} in the months between February and October, was for this reason.

- *Investigating the correlation between PM2.5 & PM10, and K_{aa} in 2014-2020*

In this subsection, the correlation between PM2.5 & PM10, and K_{aa} in 2014–2020 has been investigated. The monthly average values in Table 18 have been used. The correlation coefficients were calculated using the statistical parameter correlation coefficient, which agrees with the data for two modes (PM2.5 and K_{aa}) and two other modes (PM10 and K_{aa}) between the values in Table 18. The values for the first and second

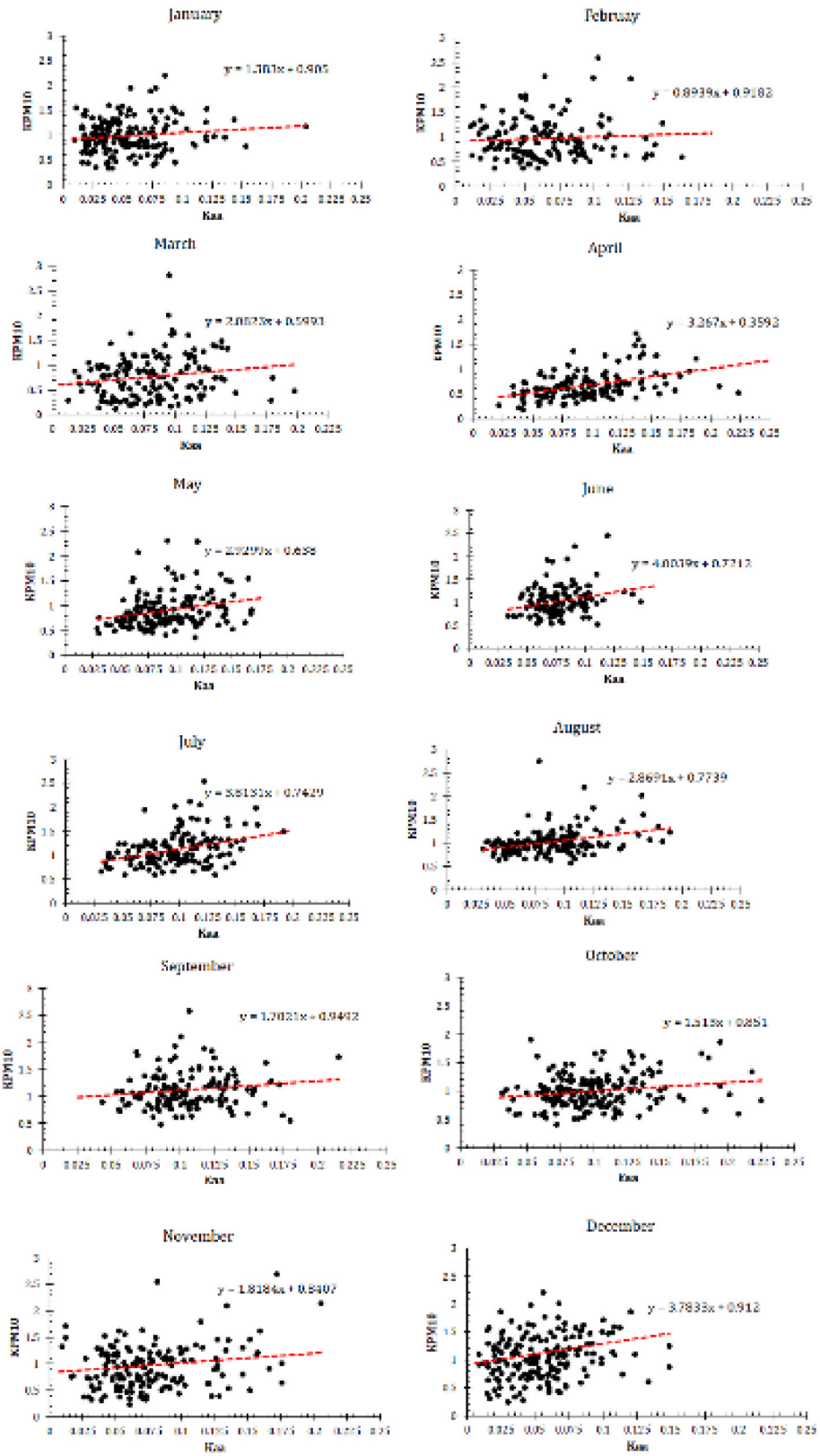

Fig. 9. The equations were fitted to the K_{aa} and K_{PM10} rearranged monthly from 2014 to 2020.

scenarios were −0.56 and 0.22, respectively. In the following subsection, this approach will be examined in detail, and twelve linear correlations will be proposed.

3.3.2. *Investigating the correlation between k_{aa} values and two parameters, $K_{PM2.5}$ and K_{PM10}, in 2014–2020*

In this part, during the years 2014–2020, we will be looking at the possible correlations that exist between the levels of K_{aa} and the parameters $K_{PM2.5}$ and K_{PM10}.

Table 20
Statistical parameters and coefficients of the fitted linear models between K_{aa} and K_{PM10} ($K_{PM10} = P1*K_{aa} + P2$).

Period	Months	Coefficients		Size	Correlation coefficients	RMSE (%)	MAPE (%)
		P1	P2				
2014–2020	January	1.383	0.905	168	0.1253	17.91	32.82
	February	0.8939	0.9182	141	0.0624	13.95	37.86
	March	2.0823	0.5993	150	0.1669	15.67	69.76
	April	3.267	0.3592	140	0.4348	16.71	32.21
	May	2.9299	0.638	151	0.2626	17.16	28.92
	June	4.0039	0.7212	126	0.2545	16.01	21.05
	July	3.8131	0.7429	153	0.3516	16.19	22.50
	August	2.8691	0.7739	154	0.3372	12.17	16.78
	September	1.7021	0.9492	151	0.1188	13.96	24.96
	October	1.513	0.851	185	0.1864	18.78	24.83
	November	1.8184	0.8407	164	0.1124	16.43	45.03
	December	3.7833	0.912	175	0.0599	19.74	41.04
	All data (average)	–	–	1858	0.2060	16.22	33.14

- *Investigating the correlations and comparing the values of K_{aa} and $K_{PM2.5}$ rearranged monthly in 2014-2020*

In this sub-section, all the data were rearranged monthly, and one linear model was fitted to the data for each month (see Fig. 8). It should be mentioned that because the PM2.5 data at the district 21 station was unavailable for several months during the seven years or was removed as an outlier, the total number of examined data pairs was 1827 (less than 2557 days of the entire period). The district 21 station was located 25 km away from the Merc radiation measurement site and was, therefore, the closest station with long-term data access.

As shown in Table 19, the slope of the fitted line - the ratio of changes in two parameters, K_{aa} and $K_{PM2.5}$—in December was 2.77. It was the maximum value of all the months. Furthermore, in this month, the maximum correlation coefficient between pairs of data was calculated at 0.2926. In this month's data, the RMSE was also at the minimum value of 9.77%.

The fitted correlations to the data are as follows. The values were reported in Table 19 (the graphs are available in **Correlation_Plots.xlsx**).

- *Investigating the correlations and comparing the values of K_{aa} and K_{PM10} rearranged monthly in 2014-2020*

In this subsection, we did the same as in the last part. All the data were clustered monthly, and a linear model was fitted to the data for each month (see Fig. 9). It should be mentioned that because the PM10 data at the district 21 station was unavailable for several months during the period or was removed as an outlier, the total number of examined data pairs was 1858 (less than 2557 days of the entire period). The district 21 station was located 25 km from the Merc radiation measurement site and represented the closest station with long-term data access. As it is shown in Table 20, the slope of the fitted line - the ratio of changes in two parameters, K_{aa} and $K_{PM2.5}$ - in June was 4.0039. It was the maximum for all months. Also, the highest value of the correlation coefficient between data pairs was calculated as 0.3516 in April.

As stated in the last sub-section, the fitted models on the data will be shown as follows. The values were reported in Table 20 (the editable graphs are available in the **Correlation_Plots.xlsx** file).

3.3.3. Summary of the investigation of the correlation between k_{aa} and two parameters, $K_{PM2.5}$ and K_{PM10}, in 2014–2020

In previous sub-sections the correlations between K_{aa} and two parameters, $K_{PM2.5}$ and K_{PM10}, in 2014–2020 were investigated, respectively. The data for the seven years was clustered monthly, and analyzed separately for each month. It is suggested to use the model with a higher correlation coefficient as needed.

As shown in Tables 19 and 20 and in the middle nine months of the year (February, March, April, May, June, July, August, September, and October) in terms of the correlation coefficient, which explains the degree of correlation, the models performed better for PM10; while in the first and last months of the year (November, December, and January), the models performed better in terms of PM2.5. This could be due to the different weather patterns in each month, which can influence the concentration of PM2.5 and PM10 in the atmosphere (Liu et al., 2020).

4. Conclusion

The monthly average PM2.5 and PM10 concentrations in Tehran experienced their lowest values in March and April of each year from 2014 to 2020, as shown in Table 9. For the month of March, the PM2.5 and PM10 values were 24.05 and 58.86 μg/m^3, respectively. Additionally, the corresponding values for April were 21.66 and 55.15 μg/m^3. It is possible to conclude that air pollution has decreased as a result of decreased automobile activity in Tehran and industry shutdowns during the official holiday (Nowruz) in March and April.

According to Table 11, the maximum daily average value of GHI radiation received in MERC in the entire period was 7961.02 W h/m^{2}d in the spring. This value was 66% higher than the entire period's average at the desired location.

In the data validation of the CERES syn 1-deg shortwave down flux all-sky condition, RMSE and MBD for validation in 2014–2020 were reported as 14.09% and 10.89%, respectively, as shown in Fig. 6. This indicates that the CERES syn 1-deg shortwave down flux all-sky condition is reliable and accurate in predicting surface solar radiation. Additionally, the results show that the model is stable and consistent over time, making it a reliable tool for climate research.

Aerosols caused 8.30% of total radiation loss from 2014 to 2020. This percentage is expected to increase in the upcoming years. The results in Table 17 showed that, the cold seasons had a 29.63% share of the total radiation reduced due to aerosols from 2014 to 2020, despite temperature inversions and PM2.5 concentration increases. This indicates that aerosols have had a more significant impact on radiation reduction in the warm seasons. This indicates that reducing aerosols in warm seasons could be an effective way to reduce the effects of climate change.

As shown in Tables 19 and 20, data was clustered monthly and analyzed separately for each month, with models dependent on PM2.5 performing better in the first and last months of the year (November, December, and January). This indicates that PM2.5 has a seasonal effect on air pollution levels. The monthly analysis also showed that PM2.5 had a greater impact on air pollution levels than other pollutants. This suggests that air pollution control policies should focus on reducing PM2.5 emissions to mitigate air pollution

CRediT authorship contribution statement

Masoud Mardani: Conceptualization, Formal analysis, Methodology, Software, Investigation, Validation, Visualization, Writing – original draft, Writing – review & editing. **Siamak Hoseinzadeh:** Conceptualization, Formal analysis, Methodology, Software, Investigation, Validation, Visualization, Project administration, Writing – original draft, Writing – review & editing, Supervision. **Davide Astiaso Garcia:** Writing – review & editing, Supervision.

Declaration of competing interest

The authors declare that they have no known competing financial interests or personal relationships that could have appeared to influence the work reported in this paper.

Data availability

Please check the attached files.

Appendix A. Supplementary data

Supplementary data to this article can be found online at https://doi.org/10.1016/j.jclepro.2023.139690.

References

Ahmad, F.A., 2018. Valuation of solar power generating potential in Iran desert areas. J. Appl. Sci. Environ. Manag. 22, 967.

Al-Hajj, R., Assi, A., Fouad, M., 2021. Short-term prediction of global solar radiation energy using weather data and machine learning ensembles: a comparative study. J. Sol. Energy Eng. 143 (5).

Alonso-Montesinos, J., et al., 2019. Intra-hour energy potential forecasting in a central solar power plant receiver combining Meteosat images and atmospheric extinction. Energy 188, 116034.

Asl-Soleimani, E., Farhangi, S., Zabihi, M.S., 2001. The effect of tilt angle, air pollution on performance of photovoltaic systems in Tehran. Renew. Energy 24 (3), 459–468.

Assareh, E., et al., 2023. A transient study on a solar-assisted combined gas power cycle for sustainable multi-generation in hot and cold climates: case studies of Dubai and Toronto. Energy 282, 128423.

Attia, A.M.A., et al., 2022. The influence of castor biodiesel blending ratio on engine performance including the determined diesel particulate matters composition. Energy 239, 121951.

Ballestrín, J., et al., 2020. Modeling solar extinction using artificial neural networks. Application to solar tower plants. Energy 199, 117432.

Bannon, P.R., 2015. Entropy production and climate efficiency. J. Atmos. Sci. 72 (8), 3268–3280.

Bannon, P.R., Lee, S., 2017. Toward quantifying the climate heat engine: solar absorption and terrestrial emission temperatures and material entropy production. J. Atmos. Sci. 74 (6), 1721–1734.

Bannon, P.R., Najjar, R.G., 2018. Heat-Engine and entropy-production analyses of the world ocean. J. Geophys. Res.: Oceans 123 (11), 8532–8547.

Bojanowski, J.S., Vrieling, A., Skidmore, A.K., 2014. A comparison of data sources for creating a long-term time series of daily gridded solar radiation for Europe. Sol. Energy 99, 152–171.

Cao, Q., et al., 2022. Country-level evaluation of solar radiation data sets using ground measurements in China. Energy 241, 122938.

Cheng, X., et al., 2022. Studies on the improvement of modelled solar radiation and the attenuation effect of aerosol using the WRF-Solar model with satellite-based AOD data over north China. Renew. Energy 196, 358–365.

Cichowicz, R., Dobrzański, M., 2022. 3D spatial dispersion of particulate matter and gaseous pollutants on a university campus in the center of an urban agglomeration. Energy 259, 125009.

Dehghani-Sanij, A., Kashkooli, F.M., 2023. Special issue: new developments and prospects in clean and renewable energies. Appl. Sci. 13 (17), 9632.

deSouza, P., et al., 2020. Air quality monitoring using mobile low-cost sensors mounted on trash-trucks: methods development and lessons learned. Sustain. Cities Soc. 60, 102239.

Di Matteo, U., et al., 2017. Energy contribution of OFMSW (Organic Fraction of Municipal Solid Waste) to energy-environmental sustainability in urban areas at small scale. Energies 10 (2), 229.

Dumka, U.C., et al., 2021. Impact of aerosol and cloud on the solar energy potential over the central gangetic himalayan region. Rem. Sens. 13 (16), 3248.

Givehchi, R., Arhami, M., Tajrishy, M., 2013. Contribution of the Middle Eastern dust source areas to PM10 levels in urban receptors: case study of Tehran, Iran. Atmos. Environ. 75, 287–295.

Global solar atlas. Available from: https://globalsolaratlas.info/.

Gómez, I., Molina, S., Galiana-Merino, J.J., 2023. Evaluating the influence of air pollution on solar radiation observations over the coastal region of Alicante (Southeastern Spain). J. Environ. Sci. 126, 633–643.

Gutiérrez, C., et al., 2018. Impact of aerosols on the spatiotemporal variability of photovoltaic energy production in the Euro-Mediterranean area. Sol. Energy 174, 1142–1152.

Hanafizadeh, P., et al., 2016. Evaluation and sizing of a CCHP system for a commercial and office buildings. J. Build. Eng. 5, 67–78.

Heger, M., 2018. Air Pollution in Tehran : Health Costs, Sources, and Policies. Environment Department Papers.

Jia, D., et al., 2022. Evaluation of machine learning models for predicting daily global and diffuse solar radiation under different weather/pollution conditions. Renew. Energy 187, 896–906.

Jiang, K., et al., 2023a. Experimental and numerical study on the potential of a new radiative cooling paint boosted by SiO2 microparticles for energy saving. Energy 283, 128473.

Jiang, H., et al., 2023b. Impact of climate changes on the stability of solar energy: evidence from observations and reanalysis. Renew. Energy 208, 726–736.

John, A., Duffie, W.A.B., 2013. Solar Engineering of Thermal Processes, fourth ed. John Wiley & Sons, Inc.

Kahan, A., 2019. EIA Projects Nearly 50% Increase in World Energy Usage by 2050, Led by Growth in Asia.

Kanase-Patil, A.B., et al., 2020. A review of artificial intelligence-based optimization techniques for the sizing of integrated renewable energy systems in smart cities. Environmental Technology Reviews 9 (1), 111–136.

Kato, S., Rose, F.G., 2020. Global and regional entropy production by radiation estimated from satellite observations. J. Clim. 33 (8), 2985–3000.

Khalesi, B., Mansouri Daneshvar, M.R., 2020. Comprehensive Temporal Analysis of Temperature Inversions across Urban Atmospheric Boundary Layer of Tehran within 2014–2018. Modeling Earth Systems and Environment.

Khan, A., Memon, S., Sattar, T.P., 2018. Analyzing integrated renewable energy and smart-grid systems to improve voltage quality and harmonic distortion losses at electric-vehicle charging stations. IEEE Access 6, 26404–26415.

Kipp & zonen sunshine duration sensor. Available from: https://www.kippzonen.com/Product/35/CSD3-Sunshine-Duration-Sensor.

Kipp. Zonen CMP22 pyranometer. Available from: https://www.kippzonen.com/Product/15/CMP22-Pyranometer.

Latitude/longitude distance calculator. Available from: https://www.nhc.noaa.gov/gccalc.shtml.

Li, P., et al., 2019. Daily surface solar radiation prediction mapping using artificial neural network: the case study of reunion Island. J. Sol. Energy Eng. 142 (2).

Li, X., Mauzerall, D.L., Bergin, M.H., 2020. Global reduction of solar power generation efficiency due to aerosols and panel soiling. Nat. Sustain. 3 (9), 720–727.

Li, R., Wang, D., Liang, S., 2021. Comprehensive assessment of five global daily downward shortwave radiation satellite products. Science of Remote Sensing 4, 100028.

Liu, Y., et al., 2007. Using aerosol optical thickness to predict ground-level PM2.5 concentrations in the St. Louis area: a comparison between MISR and MODIS. Rem. Sens. Environ. 107 (1–2), 33–44.

Liu, Z., et al., 2020. Analysis of the influence of precipitation and wind on PM2.5 and PM10 in the atmosphere. Adv. Meteorol. 2020, 5039613.

Lopes, S.M.A., Cari, E.P.T., Hajimirza, S., 2021. A comparative analysis of artificial neural networks for photovoltaic power forecast using remotes and local measurements. J. Sol. Energy Eng. 144 (2).

Luo, H., et al., 2019. Characteristics of surface solar radiation under different air pollution conditions over nanjing, China: observation and simulation. Adv. Atmos. Sci. 36 (10), 1047–1059.

Maleki, Y., Pourfayaz, F., Mehrpooya, M., 2021. Transient optimization of annual performance of a photovoltaic thermal system based on accurate estimation of coolant water temperature: a comparison with conventional methods. Case Stud. Therm. Eng. 28, 101395.

Mardani, M., 2022. Extracting Time Series from a NetCDF File Source Code.

Nabavi, S.O., Haimberger, L., Abbasi, E., 2019. Assessing PM2.5 concentrations in Tehran, Iran, from space using MAIAC, deep blue, and dark target AOD and machine learning algorithms. Atmos. Pollut. Res. 10 (3), 889–903.

Neshat, M., et al., 2023. Short-term solar radiation forecasting using hybrid deep residual learning and gated LSTM recurrent network with differential covariance matrix adaptation evolution strategy. Energy 278, 127701.

Opálková, M., et al., 2019. Influence of Air Pollution to Incident Photosynthetically Active Radiation during Clear Sky Conditions in Ostrava, Czech Republic. Atmospheric Environ. vol. 215, 116910.

Organization, W.H., 2021. WHO global air quality guidelines: particulate matter (PM2.5 and PM10), ozone, nitrogen dioxide, sulfur dioxide and carbon monoxide. In: Air Quality and Health, Centre for Environment & Health (BON), Environment, Climate Change and Health, p. 290. Guidelines Review Committee.

Prasad, A.A., Kay, M., 2021. Prediction of solar power using near-real time satellite data. Energies 14. https://doi.org/10.3390/en14185865.

Préndez, M.M., et al., 1995. Correlation between solar radiation and total syspended particulate matter in Santiago, Chile—preliminary results. Atmos. Environ. 29 (13), 1543–1551.

Rutan, D.A., et al., 2015. CERES synoptic product: methodology and validation of surface radiant flux. J. Atmos. Ocean. Technol. 32 (6), 1121–1143.

Sansaniwal, S.K., Sharma, V., Mathur, J., 2018. Energy and exergy analyses of various typical solar energy applications: a comprehensive review. Renew. Sustain. Energy Rev. 82, 1576–1601.

Sengupta, M., et al., 2021. Best practices handbook for the collection and use of solar resource data for solar energy applications. In: United States. P. Medium, third ed. Size, p. 348.
Shahsavari, A., Akbari, M., 2018. Potential of solar energy in developing countries for reducing energy-related emissions. Renew. Sustain. Energy Rev. 90, 275–291.
Su, W., Charlock, T.P., Rose, F.G., 2005. Deriving surface ultraviolet radiation from CERES surface and atmospheric radiation budget: Methodology. J. Geophys. Res. Atmos. 110 (D14).
Su, W., et al., 2007. Photosynthetically active radiation from clouds and the earth's radiant energy system (CERES) products. J. Geophys. Res.: Biogeosciences 112 (G2).
Sun, X., et al., 2022. Effects of spatial scale of atmospheric reanalysis data on clear-sky surface radiation modeling in tropical climates: a case study for Singapore. Sol. Energy 241, 525–537.
Unger, D.N., 2009. Just 5 Questions: Aerosols.
Voyant, C., et al., 2014. Time series modeling and large scale global solar radiation forecasting from geostationary satellites data. Sol. Energy 102, 131–142.
Yang, X., et al., 2016a. Distinct impact of different types of aerosols on surface solar radiation in China. J. Geophys. Res. Atmos. 121 (11), 6459–6471.
Yang, X., et al., 2016b. Intensification of aerosol pollution associated with its feedback with surface solar radiation and winds in Beijing. J. Geophys. Res. Atmos. 121 (8), 4093–4099.
Yang, D., Bright, J., 2020. Worldwide validation of 8 satellite-derived and reanalysis solar radiation products: a preliminary evaluation and overall metrics for hourly data over 27 years. Sol. Energy 210.
Yang, L., et al., 2022. Quantitative effects of air pollution on regional daily global and diffuse solar radiation under clear sky conditions. Energy Rep. 8, 1935–1948.
Zhang, C., et al., 2020. An investigation on the attenuation effect of air pollution on regional solar radiation. Renew. Energy 161, 570–578.
Zhao, Q., et al., 2019. Study on the influence of fog and haze on solar radiation based on scattering-weakening effect. Renew. Energy 134, 178–185.